Nitrogen-Doped Graphitic Nanoribbons: Synthesis, Characterization, and Transport

*Josue Ortiz-Medina, M. Luisa García-Betancourt, Xiaoting Jia, Rafael Martínez-Gordillo, Miguel A. Pelagio-Flores, David Swanson, Ana Laura Elías, Humberto R. Gutiérrez, Eduardo Gracia-Espino, Vincent Meunier, Jonathan Owens, Bobby G. Sumpter, Eduardo Cruz-Silva, Fernando J. Rodríguez-Macías, Florentino López-Urías, Emilio Muñoz-Sandoval, Mildred S. Dresselhaus, Humberto Terrones, and Mauricio Terrones**

Nitrogen-doped graphitic nanoribbons (N_x-GNRs), synthesized by chemical vapor deposition (CVD) using pyrazine as a nitrogen precursor, are reported for the first time. Scanning electron microscopy (SEM) and high-resolution transmission electron microscopy (HRTEM) reveal that the synthesized materials are formed by multilayered corrugated GNRs, which in most cases exhibit the formation of curved graphene edges (loops). This suggests that during growth, nitrogen atoms promote loop formation; undoped GNRs do not form loops at their edges. Transport measurements on individual pure GNRs exhibit a linear *I–V* (current-voltage) behavior, whereas N_x-GNRs show reduced current responses following a semiconducting-like behavior, which becomes more prominent for high nitrogen concentrations. To better understand the experimental findings, electron density of states (DOS), quantum conductance for nitrogen-doped zigzag and armchair single-layer GNRs are calculated for different N doping concentrations using density functional theory (DFT) and non-equilibrium Green functions. These calculations confirm the crucial role of nitrogen atoms in the transport properties, confirming that the nonlinear *I–V* curves are due to the presence of nitrogen atoms within the N_x-GNRs lattice that act as scattering sites. These characteristic N_x-GNRs transport properties could be advantageous in the fabrication of electronic devices including sensors in which metal-like undoped GNRs are unsuitable.

1. Introduction

The rise of graphene, a unique one atom-thick carbon nanomaterial, has led to extensive efforts aimed at developing applications based on their exceptional electronic properties: zero-gap semiconducting band structure, a high charge carrier mobility and quantum Hall effect.[1,2] However, for finite graphene sheets, the electronic behavior becomes more complex due to the presence of edge effects. This becomes evident in semi-infinite sheets that extend continuously in one direction but are restricted to a finite width along the other, also known as graphene-nanoribbons (graphene-NRs). Fujita et al.[3] were the first using tight binding calculations to predict the electronic properties of graphene-NRs; more recently, detailed

J. Ortiz-Medina, M. L. García-Betancourt, Dr. E. Garcia-Espino, Prof. F. J. Rodríguez-Macías, Prof. F. López-Urías, Prof. E. Muñoz-Sandoval
Advanced Materials Department
IPICYT, Camino a Presa San José 2055, Lomas 4a sección
San Luis Potosí 78216, México

J. Ortiz-Medina, M. L. García-Betancourt, Dr. A. L. Elías, Dr. H. R. Gutiérrez, Prof. F. López-Urías, Prof. H. Terrones, Prof. M. Terrones
Department of Physics,The Pennsylvania State University
University Park, PA 16802, USA
E-mail: mut11@psu.edu

Dr. X. Jia
Department of Materials Science and Engineering
Massachusetts Institute of Technology
Cambridge, MA 02139, USA

R. Martínez-Gordillo
Centre d'Investigació en Nanociència i Nanotecnologia (CSIC-ICN)
Campus de la UAB, E-08193 Bellaterra, Spain

M. A. Pelagio-Flores, Prof. F. J. Rodríguez-Macías
Departamento de Química Fundamental
Universidade Federal de Pernambuco
50740-540 Recife, PE, Brazil

D. Swanson
Chemistry and Physics Departments
Augustana College
Sioux Falls, SD 57197, USA

Dr. V. Meunier, Dr. B. G. Sumpter, Dr. E. Cruz-Silva
Oak Ridge National Laboratory
Oak Ridge, TN 37831, USA

Dr. V. Meunier, J. Owens
Department of Physics, Applied Physics and Astronomy
Rensselaer Polytechnic Institute
Troy, NY 12180-3590, USA

Prof. M. Dresselhaus
Department of Electrical Engineering and Computer Science
Massachusetts Institute of Technology
Cambridge, MA 02139, USA

Prof. M. Dresselhaus
Department of Physics
Massachusetts Institute of Technology
Cambridge, MA 02139, USA

Prof. M. Terrones
Shinshu University, Research Center for Exotic Nanocarbons
Nagano 3808553, Japan

DOI: 10.1002/adfm.201202947

theoretical models have been constructed and explored.[4–6] These calculations established that for graphene-NRs with armchair edges, the system could be a semimetal or a semiconductor, whereas zigzag edges produce a metallic-like behavior due to the presence of localized states at the Fermi level.[7,8] When considering spin polarization both systems become semiconductors.[9]

Efforts in tailoring the physico-chemical properties of GNRs, which comprise several layers of graphene, have led to different approaches including the introduction of different types of defects in the graphene lattice in order to alter significantly its electronic structure. In this context, the introduction of foreign atoms within the carbon lattice of graphene-NRs[10] directly impacts their electronic properties; the excess or lack of charge carriers would result in either n- or p-type transport. It is noteworthy that changes in the electronic properties of carbon nanotubes (CNTs) by doping with either nitrogen or boron have been demonstrated previously.[8,11] However, experimental research related to doped graphene and graphitic nanoribbons remains under intense investigation. From the experimental standpoint, various groups have reported the synthesis of undoped graphene and graphene-NRs using: 1) chemical coupling,[12] 2) CVD,[13,14] 3) graphene nanocutting,[15,16] 4) CNTs exfoliation,[17] and 5) unzipping.[18–20] Other groups have recently developed successful approaches to dope flat and extended sheets of graphene.[21] For instance, a CVD method for growing few-layer graphene on Cu films was reported by Wei and collaborators, demonstrating effective nitrogen doping of flat sheets.[22] More recently, Brenner and Murali proposed an in situ doping method driven by graphite exfoliation under N_2,[23] whereby nitrogen passivates the dangling bonds that form at the edges as the ribbon exfoliates from graphene sheets. Wang et al. reported the introduction of nitrogen atoms at the graphene-NRs edges by Joule heating in the presence of gaseous ammonia,[24] resulting in nitrogen functionalization at the edges, achieving an n-type electronic doping.

Changes in electron transport are clearly among the most direct consequences of doping carbon nanostructures, and doping has been mainly explored theoretically for CNTs[25,26] and graphene.[6,10,21,22] Nitrogen doping could result in either n- or p-type semiconducting behavior, depending on the type and position of the nitrogenated sites (i.e., substitutional, pyridine-like or pyrrolic nitrogen).[27,28] The doping of graphene-NRs, in conjunction with approaches such as band gap tuning by electric fields in bilayer graphene[29,30] and graphene nanoribbon edges design[31,32] are commonly explored as alternatives for graphene band gap engineering. However, practical approaches for bulk synthesis of graphene and GNRs ribbons with semiconducting characteristics are still troublesome.

In this work, we report the successful synthesis of large quantities of N_x-GNRs by aerosol assisted chemical vapor deposition (AA-CVD). The nitrogen doping in the ribbon samples is controlled by modifying pyrazine concentration in the precursor solution used as feedstock during the CVD process. Characterization techniques such as scanning electron microscopy (SEM), high-resolution transmission electron microscopy (HRTEM), Raman and X-ray photoelectron (XPS) spectroscopies, thermogravimetric analysis (TGA), and electrical measurements are reported. In addition, density functional theory (DFT) calculations are performed in order to compare, and understand better, the experimental transport found in the samples. We note that the N_x-GNRs exhibit loop formations at the ribbon edges, an increased chemical reactivity and a novel semiconducting-like behavior, all caused by the nitrogen doping. To the best of our knowledge, this is the first single-step synthesis method for producing N_x-GNRs with such advantageous characteristics.

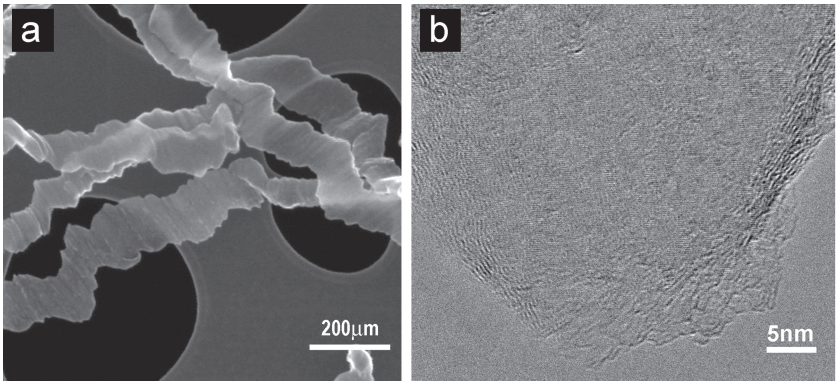

Figure 1. a) SEM and b) TEM images of undoped graphitic nanoribbons. The morphological characteristics observed by SEM reveal a rippled surface and high aspect ratio.

2. Results and Discussion

Figure 1 depicts SEM and HRTEM images of pristine (and undoped) GNRs. The ribbons exhibit several layers and rippled (corrugated) surfaces, same as those previously synthetized by Campos-Delgado et al.[13] SEM images of the N-doped synthesized samples are shown in **Figure 2**. The latter correspond to N_x-GNRs produced using different pyrazine concentrations. For all concentrations used, N_x-GNRs show high aspect ratio (lengths of few microns against widths going from 50 to 500 nm), and overall shapes similar to undoped GNRs.[13] The main difference observed is that thicker and less rippled N_x-GNRs are seen when adding more pyrazine to the precursor solution. **Figure 3** depicts HRTEM images, showing the ribbons' multilayered nature. TEM shows average thicknesses of 30–40 nm, indicating that N_x-GNR have ≤100 graphene sheets, a value much larger when compared to undoped GNRs. Interestingly, the edges of N_x-GNRs exhibit loops (coalesced adjacent graphene sheets, see Figure 3f). From all the observed loop configurations in the N_x-GNRs, it is possible to identify three types of edge morphologies: a) "multilayered" loops, where several layers "fold" in a concentric fashion (see Figure 3b,h); b) individual or "single-layered" loops, which join two adjacent graphene edges (see Figure 3f); and c) quasi-closed or "open" loops in which various layers bend together (see Figure 3g,h). All loop types appears for all doped N_x-GNRs, but the multilayered and "open" loops are found more frequently for the high pyrazine concentrations.

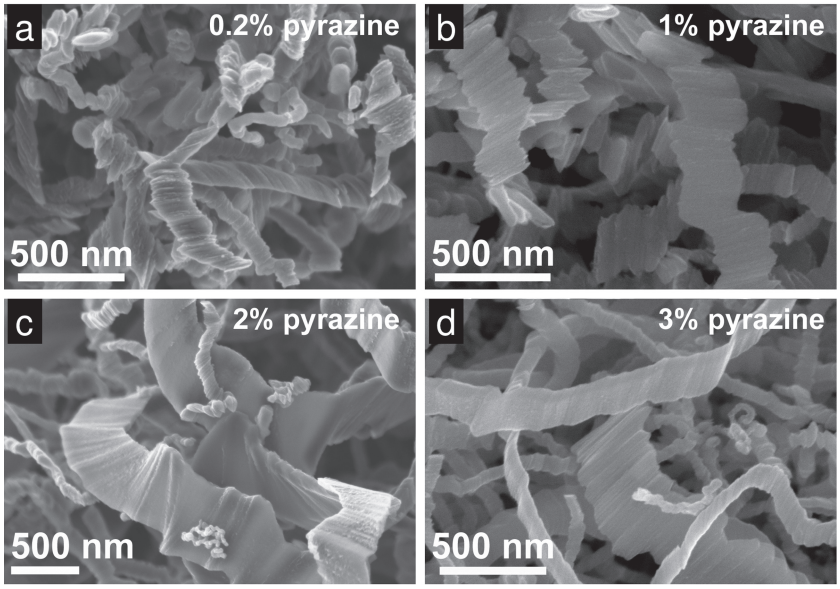

Figure 2. SEM images of nitrogen-doped graphitic nanoribons (N_x-GNRs) synthesized using aerosol-assisted chemical vapor deposition (AA-CVD) method; with different concentrations of the nitrogen containing precursor, pyrazine ($C_4H_4N_2$): a) 0.2 wt%, b) 1.0 wt%, c) 2.0 wt%, and d) 3.0 wt% The ripples are less pronounced and wider nanoribbons are obtained with higher pyrazine concentrations.

It is important to note that as-synthesized undoped GNRs do not show these loops, and they could only be observed after a subsequent high temperature (above 2000 °C) treatment in an Ar atmosphere.[33,34] Therefore, the loops observed in N_x-GNRs might be different in nature, since they are produced during the CVD at lower temperatures (950 °C). We believe these loops are stabilized by the presence of nitrogen atoms at highly curved regions.

Raman spectroscopy data reveal important changes associated with the nitrogen doping of the N_x-GNRs. **Figure 4**a,b depict the Raman spectra showing the D-, G-, D′- and G′-bands, corresponding to N_x-GNRs and undoped GNRs. The D- and G-bands for pristine GNRs are localized around 1351 cm^{-1} and 1581 cm^{-1}, respectively, and the D- and G-band intensity ratio (I_D/I_G) of 1.07 (see Figure 4e) is similar to previously reported work.[13] For N_x-GNRs, the observed spectra suggest changes caused by charge transfer effects of nitrogen atoms and the presence of "disordered" or non sp^2 hybridized carbon atoms. Figure 4c,d show N_x-GNRs' D-, G-, D′- and G′ (2D)-band shifts caused by the introduction of nitrogen within the carbon system. It is noticeable that even though the shifts' magnitude is relatively small, the trend, especially for the D′- and G′-bands, is consistent with an increase in the nitrogen concentration. Figure 4e reveals the peak intensity ratios associated with the presence of non sp^2 hybridized carbon, displaying the contribution of nitrogen doping regions. However, it is difficult to attribute increases of D-band intensities only to the presence of nitrogen, since the undoped GNRs exhibit similar ratios due to the presence of bare edges and rippled morphologies.[13] Interestingly, a clear decrease in the intensity ratio could be observed for the G′-band (see Figure 4f) as the nitrogen precursor concentration increases. This observation is in agreement with previous reported phenomena on electrically and chemically doped

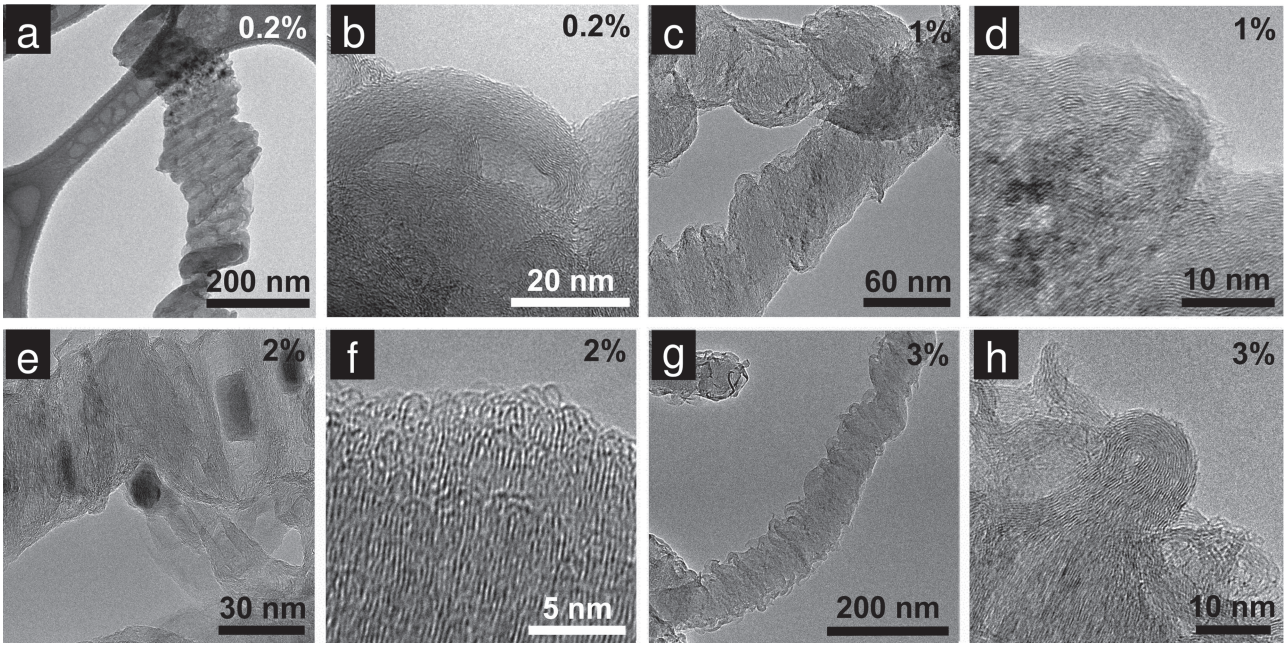

Figure 3. TEM images of N_x-GNRs synthesized by AA-CVD. Each consecutive pair corresponds to a different pyrazine concentration as nitrogen precursor: a,b) 0.2 wt%, c,d) 1.0 wt%, e,f) 2.0 wt%, and g,h) 3.0 wt%. The higher magnification images show different loop configurations for the edges.

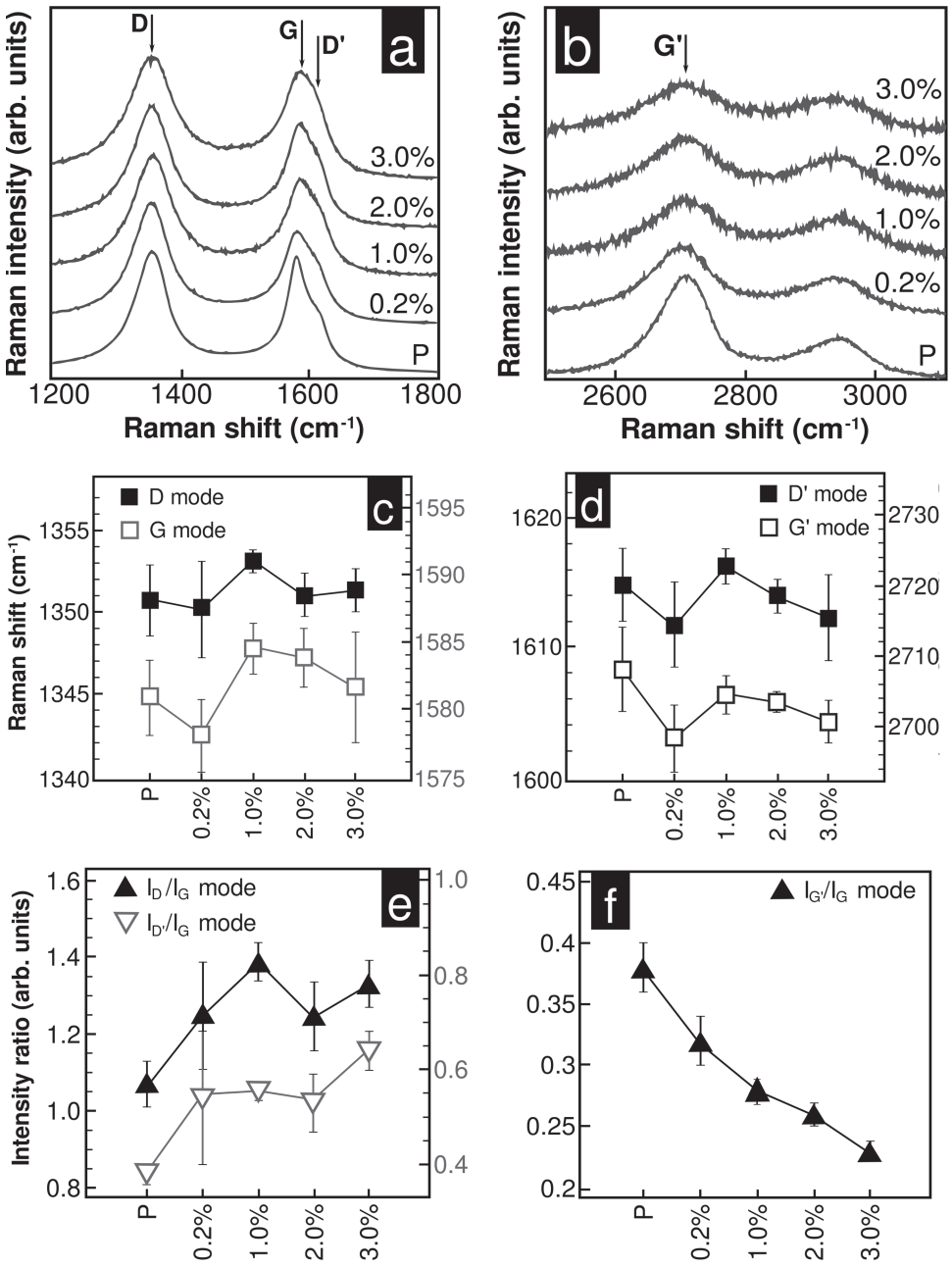

Figure 4. Raman spectra for N_x-GNRs, including the undoped or pristine case (labeled as P) for comparison. a) shows the region of the D, G and D′ Raman modes, where the doping causes changes in the shape of the G-D′ peaks and b) the regions of G′ Raman mode where changes in the intensity in the G′ peaks are observed. The arrows in (a,b) indicate the average peak positions associated with each Raman mode. c,d) Raman shifts for the four modes, showing a weak downshifting trend for high nitrogen concentrations. e,f) Raman intensity ratios. The I_D/I_G ratio is associated with non-sp^2 bonding points. The $I_{G'}/I_G$ ratio shows a correlation to the pyrazine concentration. The error bars on (c–f) denote one standard deviation.

graphene,[35–37] where the$I_{G'}/I_G$ ratio changes are correlated with the doping level.

X-ray photoelectron spectroscopy (XPS) confirms the presence of nitrogen within our N_x-GNRs. N1s line scans of the samples synthesized with the three higher pyrazine concentrations are shown in **Figure 5**a; for lower nitrogen precursor concentrations the N1s signal was below the detection limit of the XPS instrument. These XPS analysis revealed nitrogen doping levels of 0.08 at%, 0.30 at% and 0.28 at% (with ±30% error), for samples synthesized using 1%, 2% and 3% of pyrazine, respectively. These values are lower than the concentrations reported for other N-doped carbon nanomaterials synthesized by CVD.[27,38,39] It is important to note that the final dopant concentration has a strong dependence on the synthesis method and parameters used, such as temperature, synthesis times, and type of precursors. The XPS results also reveal that the preponderance of N doping is substitutional and in adequate quantity to produce electronic scattering events but

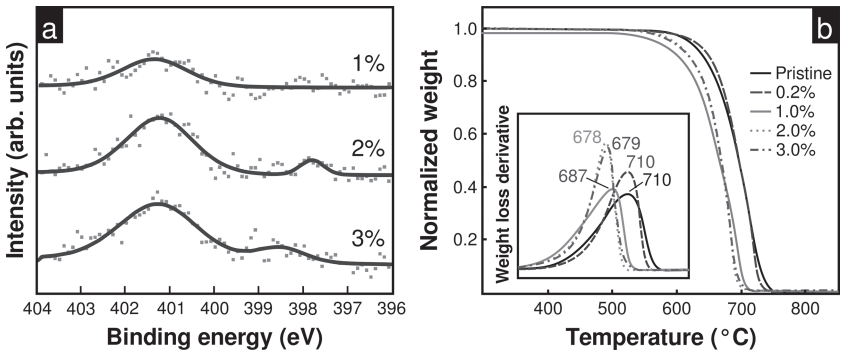

Figure 5. a) XPS N(1s) spectra for N_x-GNRs synthesized with 1.0%, 2.0% and 3.0% of pyrazine in the precursor mixture. b) TGA plots for all the N_x-GNRs samples, and undoped GNRs. The inset plots the first derivative of weight loss, and shows the respective thermal degradation critical temperature. Note the reduced thermal stability for N_x-GNRs with high N concentrations.

insufficient to yield a clear n-type doping. Although the amount of nitrogen atoms was close to the equipment's detection limit, broad peaks around 401.4 eV are clearly observed. These are associated with substitutional nitrogen doping (three coordinated nitrogen atoms within the graphene lattice).[22] For the 2.0% and 3.0% pyrazine samples, there is no significant difference in the measured doping level, possibly indicating a nitrogen saturation within the graphene sheets. A similar trend has been found in the N-doped single-walled carbon nanotubes (SWNTs), in which the nitrogen precursor (e.g., benzylamine) reveals a saturation effect at a given concentration within the precursor solution.[40]

Thermogravimetric analysis (TGA) curves and their first derivatives for pristine and N_x-GNRs are shown in figure 5b. These results indicate that there is a maximum level of doping within N_x-GNRs, which is reached when using 2% pyrazine. For both 2% and 3% pyrazine N_x-GNRs, the onset of combustion is 30 °C lower than the pristine counterparts, and with a higher burning rate (1.7 and 1.6 times faster, respectively). For 1% pyrazine, the N_x-GNRs decompose 23 °C earlier than the pristine GNRs, and reveal a similar burning rate. The samples obtained using 0.2 wt% pyrazine in the solution have the same critical degradation temperature when compared to pristine GNRs, but show a higher burning rate (1.3 times). Such results are explained by increasing the nitrogen concentrations within N_x-GNRs; nitrogen atoms promote reactions with oxygen. This effect is not only qualitatively similar to N-doped multiwalled carbon nanotubes (CN_x -MWNTs), but CN_x-MWNTs and N_x-GNRs critical degradation temperatures match, according to results found in the literature.[41]

Electrical measurements performed on individual N_x-GNRs revealed clear differences when compared to pristine GNRs. **Figure 6**a shows that the current–voltage (*I–V*) curves for individual undoped GNRs have a purely ohmic behavior (with a resistance of 25 KΩ); whereas for 0.2% pyrazine N_x-GNR, a variable-resistivity curve is always observed. The resistivity is around 715 KΩ for 100 mV of applied voltage and decreases to around 85 KΩ at 900 mV of applied voltage. For the 3% pyrazine N_x-GNR, the change in resistivity goes from 2.38 MΩ at 100 mV to 230 KΩ at 900 mV. The experimental results suggest that the changes in transport reflect the correspondent modification in the conductive regime due to the diffusive electronic transport nature produced by the scattering sites (mainly induced by nitrogen atoms).[42]

Figure 6b shows that successive *I–V* measurements on a single N_x-GNR (shown in the inset), induce a slight curve linearization. This could be attributed to the annealing (induced by Joule heating) of edges and defects, in which substitutional nitrogen atoms are being removed from the carbon network. For pristine GNRs, the *I–V* curve is always linear, and the conductivity enhances after annealing; defect removal due to Joule heating has been reported in the literature.[43]

In order to understand the role of the nitrogen doping in carbon nanoribbons, DFT calculations were performed on zigzag and armchair nanoribbons. **Figure 7** depicts spin-up and spin-down density of states (DOS) and quantum conductance for zigzag (18-zGNRs) nanoribbons and the corresponding molecular models, with the doping level expressed as a percentage of substitutional nitrogen atoms with respect to carbon. For zGNRs systems (see Figure 7), increasing nitrogen concentration has a visible effect in the nanoribbons' conduction band, introducing localized states (seen as sharp peaks in DOS plots) that act as electronic scattering points. For the aGNRs the calculations reveal similar effects to those seen for zGNRs (see Supporting Information, Figure S1); a clear reduction in the number of states above the Fermi level. These results agree with previous theoretical studies of quantum conductivity of nitrogen-doped nanocarbons,[5,10,11] in which the conductivity drop is rationalized as being due to donor- or acceptor-like

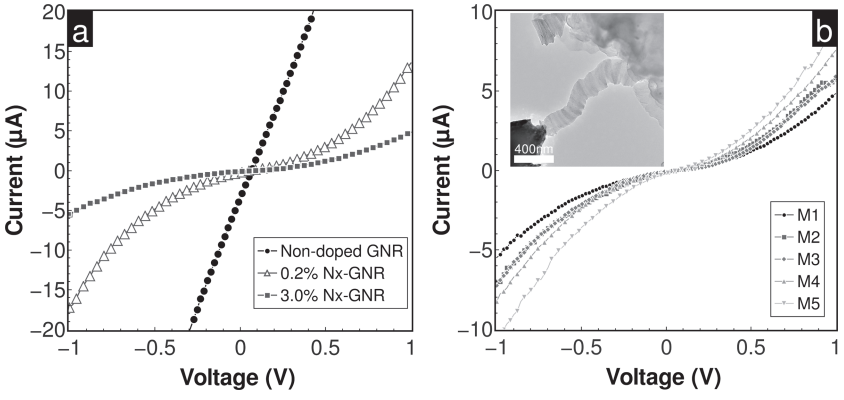

Figure 6. Measured electrical transport results for individual N_x-GNRs. a) *I–V* measurement curves for pristine (GNR) and for 0.2% and 3.0% pyrazine N_x-GNRs. Note that the doped nanoribbons exhibit a semiconducting-like behavior. b) Resistance linearization produced by the Joule heating effect, after consecutive *I–V* measurements (labeled M1, M2, …, M5) on a single N_x-GNR (3.0% pyrazine, see TEM image in the inset). Even when the resistance is lower, the semiconducting-like behavior remains.

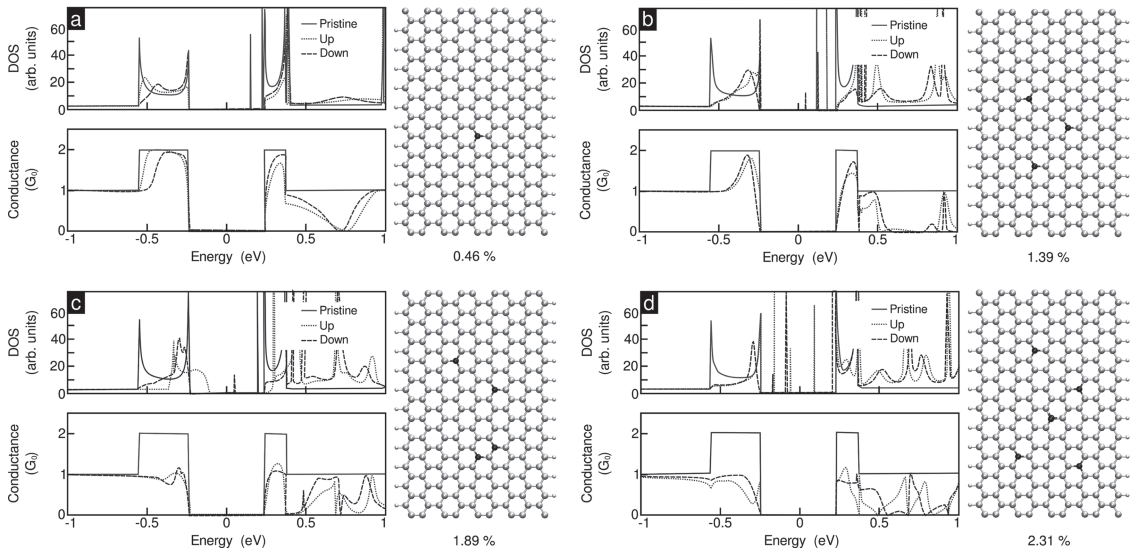

Figure 7. DOS, conductance (spin-up and spin-down), and visualizations of 18-zGNRs doped with a) one, b) three, c) four, and d) five nitrogen atoms. The solid line represents the DOS and conductance for a pristine (undoped) 18-zGNR for comparison, as explained in the text the spin-up and spin-down DOS are the same for undoped GNR and only one curve is shown. The percentages represent the number of nitrogen atoms divided by the total atoms (excluding the passivating hydrogens on the edges). The quantum conductance is given in G_0 units ($G_0 = 2e^2/h$).

localized states (seen as flat bands on the nanoribbons' band structure), induced by the extra electron carried by the nitrogen. Most importantly, these results are in good agreement with our experimental results, in which N_x-GNRs have lower conductivity values when compared to undoped GNRs.

It is noteworthy that our calculations were carried out using spin-polarization, which provide the most stable (minimal energy) magnetic ordering structure for undoped zigzag nanoribbons and were also used for N-doped nanoribbons. The undoped ribbons exhibit localized magnetic moments along the edges, with both edges exhibiting a ferromagnetic order (aligned spins along the edges) with opposite spin direction between edges resulting in a zero total magnetization, thus in the DOS figures there is no noticeable effect of spin-polarization and only one line is shown. Given that there is an electronic band gap in both zigzag and armchair nanoribbons (see Figure 7 and Supporting Information Figure S1), the corresponding spin-resolved *I–V* curves (shown in Supporting Information Figure S2) exhibit a turn-on voltage of ≈0.3 V for the undoped GNR, which contradicts the experimental evidence (Figure 6a). When non-spin polarized calculations are performed, zigzag graphene-NRs exhibit a zero electronic band gap. The energy differences between spin-polarized and non-spin polarized calculations are of the order of meV, and decrease with nanoribbon's width. Therefore, we expect that at room temperature, the spins do not play an important role in the transport properties of these graphitic carbon nanoribbons. **Figure 8** depicts the calculated *I–V* curves between the electrodes (non-polarized calculations), where the linear *I–V* curve exhibited by undoped nanoribbons qualitatively agrees with our experimental measurements (Figure 6a).

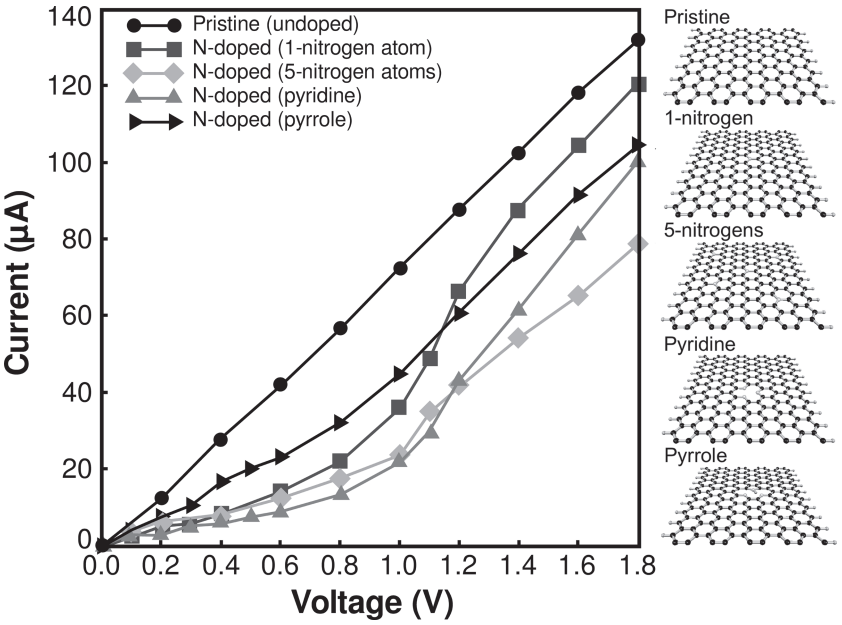

Figure 8. Electrical current as a function of the applied voltage for nitrogen-doped and undoped (pristine) zigzag graphene nanoribbons (18-zGNRs). The calculations were carried out with non-spin polarized local density approximation. The nanoribbons were doped in a substitutional, pyridine or pyrrole fashion. In the pyridine and pyrrole doping, one carbon atom is removed (in our case, it was removed for the central part of nanoribbon) and the carbon atoms around the vacancy are replaced by nitrogen atoms. The corresponding structures of the considered cases are shown in the right side of the figure.

At any of the nitrogen doping cases considered, both substitutional and pyridine-type, the *I–V* behavior of N-doped graphene nanoribbons is non-linear, and it shows a semiconducting-like behavior. Similarly to the experimental results, the calculations also show that increased doping levels increase the resistivity. We therefore believe that nitrogen atoms embedded within our N_x-GNRs enables attractive semiconducting properties, which could be useful for graphene-based nanoelectronic devices.

3. Conclusions

In summary, we have successfully synthesized bulk quantities (hundreds of milligrams) of N_x-GNRs by AA-CVD. The novel morphological features observed in these structures consist of loops located at the nanoribbons edges, induced by the presence of nitrogen atoms during synthesis; the N_x-GNRs also possess increased reactivity at high temperatures (as verified by the lower decomposition temperatures in TGA). Therefore, the N_x-GNRs might be easily functionalized, thus enabling applications related to the fabrication of composite materials, molecular sensors, field emitters, etc. Both TGA and XPS suggest that there is a threshold limit value of nitrogen atoms capable of being incorporated in doped GNRs. Detailed characterization studies of the N_x-GNRs by Raman spectroscopy indicate that the intensity ratio between the G′ and G peaks ($I_{G'}/I_G$) is correlated to the nitrogen doping concentration. Electrical measurements on individual GNRs showed electronic transport differences between the N_x-GNRs and undoped nanoribbons. Theoretical calculations suggest that the nitrogen doping introduces electron scattering and that is largely responsible for the semiconducting-like features observed in N_x-GNRs. Further theoretical calculations considering the effect of loop formation and the stacking of different layers in the graphitic nanoribbons are still under investigation in order to better understand these doped nanocarbons. These new types of doped GNRs possess different properties when compared to pristine GNRs, thus making this material attractive for the fabrication of electronic nanodevices.

4. Experimental Section and Theoretical Details

N_x-GNRs Synthesis: The N-doped nanoribbons were synthesized by AA-CVD as reported elsewhere.[13] This approach involved the pyrolysis of an ethanol (C_2H_5OH) solution of thiophene (C_4H_4S, 0.097%v/v), ferrocene ($C_{10}H_{10}Fe$, 1% wt/vol), and pyrazine ($C_4H_4N_2$). Different pyrazine concentrations in the solution were used (0.0%, 0.2%, 1.0%, 2.0% and 3.0% wt/vol, for further reference). The AA-CVD experiments were carried out at 950 °C for 30 min under an inert atmosphere (Ar 0.8 L min^{-1}). The resulting material was collected from the reaction quartz tube by scraping its inner walls in the region corresponding to the center of the tubular furnace.

Electron Microscopy: SEM (Leo 1530 FE-SEM, 2 KV) and HRTEM (Jeol 2010, 200 KV) were used for morphological characterization of N_x-GNRs. For SEM, small amounts of as-synthesized material were deposited on carbon tape over Al pins. For HRTEM, small amounts of the powder samples were ultrasonicated in isopropyl alcohol and deposited on Cu holey carbon TEM grids.

Spectroscopy: As synthesized samples were analyzed with a Renishaw microRaman spectrometer, with a 514 nm excitation laser wavelength. The nitrogen content in the N_x-GNRs samples was measured by XPS (Kratos Axis Ultra XPS). Survey scans (not shown here) were obtained only for the three samples with the largest nitrogen concentrations (1.0 wt%, 2.0 wt%, and 3.0 wt% pyrazine in the precursor solution), including the N1s and C1s high-resolution spectra.

Thermogravimetric Analysis: Approximately 2.5 mg of each analyzed sample were heated at 10 °C min^{-1}, in a TA-Q5000IR, with a 2.5 L min^{-1} dry air flux.

Electrical Measurements: In order to experimentally assess the electronic transport, room temperature (T = 300 K) *I–V* measurements were performed on individual N_x-GNRs, and undoped GNRs for comparison. Individual nanoribbons were connected between metallic electrodes inside a transmission electron microscope, a sweeping DC voltage (–1.0 to 1.0 V) was applied, and the resulting current was measured.

DFT Calculation Details: Electronic calculations were performed using DFT as implemented in the SIESTA code.[44] Generalized gradient approximation (GGA) functionals using the Perdew-Burke-Ernzerhof implementation were used for all calculations.[45] The basis set was made up of double-ξ with single polarization orbitals, with an energy shift of 50 meV. A zigzag graphene-NR with 18 atoms along the width (18-zGNR, width w = 1.99 nm, length l = 2.84 nm) and an armchair GNR (14-aGNR, w = 1.79 nm, l = 2.42 nm) with different amounts and configurations of dopant nitrogen atoms was used to investigate the electron transport as a function of the nitrogen doping. Twelve and six unit cells were considered in the calculations for zGNRs and aGNRs, respectively. A real-space mesh equivalent to a plane-wave cutoff energy of 250 Ry for real-space integrals was used. The Brillouin zone was sampled using a Monkhorst-Pack grid corresponding to four and one *k*-points, for zGNR and aGNR, respectively, in the transport direction. Vacuum distances of 18 Å were kept between the graphene nanoribbons in the finite directions. All graphene-NRs were passivated with hydrogen on the edges in order to increase thermodynamic stability[46] and the coordinates of all systems were relaxed using conjugate gradient minimization until the maximum force was less than 0.05 eV $Å^{-1}$.

For zGNR doping C atoms in the nanoribbon center were replaced with 1, 3, and 5 (in two different configurations) nitrogen atoms. The aGNR were doped by the substitution of one (both on the center or edge) and five nitrogen atoms. Starting with the relaxed atomic structure and the converged Hamiltonian and overlap matrices, all obtained from SIESTA,[44] conductance and DOS calculations were performed using our in-house transport code based on the Landauer-Buttiker formalism outlined by Datta[47] and used in previous similar studies.[48–51] In all three doping schemes, the electrodes used were those obtained from the pristine SIESTA calculation. An electrode consists of one aGNR or two zGNR unit cells on each end of the system. Results were obtained for both spin-up and spin-down electrons in the doped cases; for the pristine (undoped) structure the electron conductance was invariant between spin-up and spin-down. For energy stability, the nanoribbons are studied in the antiferromagnetic configuration.[52] The *I–V* curves were obtained using simple ξ orbitals and TRANSIESTA calculations.[53]

Supporting Information

Supporting Information is available from the Wiley Online Library or from the author.

Acknowledgements

M.T. thanks JST-Japan for funding the Research Center for Exotic NanoCarbons, under the Japanese regional Innovation Strategy Program by the Excellence. M.T. is grateful to the Penn State Center for Nanoscale Science (MRSEC; NSF grant number DMR-0820404), for a seed grant on "Defect Engineering in Layered Materials". H.T. acknowledges support of CAPES, Brazil, through its Foreign Scientist Invited program. F.J.R.M., F.L.U., and E.M.S. acknowledge CONACYT (México) grants

CB-2008-SEP-107082, 60218-F1 and 48300 S-3907, respectively. X.J. and M.S.D. acknowledge the MURI grant ONR-N00014-09-1-1063. R.M.G. was supported by MCINN, project number FIS2009-12721-C04-01 and scholarship AGAUR "FI-DGR 2011". This work was supported by CONACYT Ph.D. scholarships 223807 (J.O.M.) and 223824 (M.L.G.B.), as well as financial research support from PSU. J.O.M. thanks complementary support from the Graduate Complementary Scholarship program (DGRI-SEP, México). B.G.S. was supported by the Center for Nanophase Materials Sciences (CNMS), sponsored at Oak Ridge National Laboratory by the Division of Scientific User Facilities, U.S. Department of Energy.

Received: October 10, 2012
Revised: January 25, 2013
Published online: March 19, 2013

[1] K. S. Novoselov, D. Jiang, F. Schedin, T. J. Booth, V. V. Khotkevich, S. V. Morozov, A. K. Geim, *Proc. Natl. Acad. Sci. USA* **2005**, *102*, 10451.
[2] A. K. Geim, K. S. Novoselov, *Nat. Mater.* **2007**, *6*, 183.
[3] M. Fujita, K. Wakabayashi, K. Nakada, K. Kusakabe, *J. Phys. Soc. Jpn.* **1996**, *65*, 1920.
[4] B. Biel, F. Triozon, X. Blase, S. Roche, *Nano Lett.* **2009**, *9*, 2725.
[5] S. Yu, W. Zheng, Q. Wen, Q. Jiang, *Carbon* **2008**, *46*, 537.
[6] T. Martins, R. Miwa, A. da Silva, A. Fazzio, *Phys. Rev. Lett.* **2007**, *98*, 196803.
[7] L. Brey, H. A. Fertig, *Phys. Rev. B* **2006**, *73*, 235411.
[8] K. P. Loh, Q. Bao, P. K. Ang, J. Yang, *J. Mater. Chem.* **2010**, *20*, 2277.
[9] Y.-W. Son, M. L. Cohen, S. G. Louie, *Phys. Rev. Lett.* **2006**, *97*, 216803.
[10] E. Cruz-Silva, Z. M. Barnett, B. G. Sumpter, V. Meunier, *Phys. Rev. B* **2011**, *83*, 155445.
[11] J. C. Charlier, P. C. Eklund, J. Zhu, A. C. Ferrari, in *Topics in Applied Physics*, Vol. *111*, (Ed: A. Jorio, G. Dresselhaus, M. S. Dresselhaus), Springer-Verlag GmbH, Heidelberg, Germany **2008**, pp. 673–709.
[12] J. Cai, P. Ruffieux, R. Jaafar, M. Bieri, T. Braun, S. Blankenburg, M. Muoth, A. P. Seitsonen, M. Saleh, X. Feng, K. Mullen, R. Fasel, *Nature* **2010**, *466*, 470.
[13] J. Campos-Delgado, J. M. Romo-Herrera, X. Jia, D. A. Cullen, H. Muramatsu, Y. A. Kim, T. Hayashi, Z. Ren, D. J. Smith, Y. Okuno, T. Ohba, H. Kanoh, K. Kaneko, M. Endo, H. Terrones, M. S. Dresselhaus, M. Terrones, *Nano Lett.* **2008**, *8*, 2773.
[14] P. Mahanandia, K. Nanda, V. Prasad, S. Subramanyam, *Mater. Res. Bull.* **2008**, *43*, 3252.
[15] L. Ci, L. Song, D. Jariwala, A. L. Elías, W. Gao, M. Terrones, P. M. Ajayan, *Adv. Mater.* **2009**, *21*, 4487.
[16] L. Ci, Z. Xu, L. Wang, W. Gao, F. Ding, K. Kelly, B. Yakobson, P. Ajayan, *Nano Res.* **2008**, *1*, 116.
[17] A. G. Cano-Márquez, F. J. Rodríguez-Macías, J. Campos-Delgado, C. G. Espinosa-González, F. Tristán-López, D. Ramírez-González, D. A. Cullen, D. J. Smith, M. Terrones, Y. I. Vega-Cantú, *Nano Lett.* **2009**, *9*, 1527.
[18] M. S. Meier, J. P. Selegue, K. B. Cassity, A. P. Kaur, D. Qian, *J. Phys.: Condens. Matter* **2010**, *22*, 334219.
[19] L. Jiao, L. Zhang, L. Ding, J. Liu, H. Dai, *Nano Res.* **2010**, *3*, 387.
[20] A. L. Elías, A. R. Botello-Méndez, D. Meneses-Rodríguez, V. Jehová González, D. Ramírez-González, L. Ci, E. Muñoz-Sandoval, P. M. Ajayan, H. Terrones, M. Terrones, *Nano Lett.* **2009**, *10*, 366.
[21] H. Liu, Y. Liu, D. Zhu, *J. Mater. Chem.* **2011**, *21*, 3335.
[22] D. Wei, Y. Liu, Y. Wang, H. Zhang, L. Huang, G. Yu, *Nano Lett.* **2009**, *9*, 1752.
[23] K. Brenner, R. Murali, *Appl. Phys. Lett.* **2011**, *98*, 113115.
[24] X. Wang, X. Li, L. Zhang, Y. Yoon, P. K. Weber, H. Wang, J. Guo, H. Dai, *Science* **2009**, *324*, 768.
[25] S. Latil, S. Roche, D. Mayou, J. C. Charlier, *Phys. Rev. Lett.* **2004**, *92*, 256805.
[26] J. Wei, H. Hu, H. Zeng, Z. Zhou, W. Yang, P. Peng, *Physica E* **2008**, *40*, 462.
[27] R. Czerw, M. Terrones, J. Charlier, X. Blase, B. Foley, R. Kamalakaran, N. Grobert, H. Terrones, D. Tekleab, P. M. Ajayan, W. Blau, M. Rühle, D. L. Carroll, *Nano Lett.* **2001**, *1*, 457.
[28] M. Zhao, Y. Xia, J. P. Lewis, R. Zhang, *J. Appl. Phys.* **2003**, *94*, 2398.
[29] E. McCann, D. S. Abergel, V. I. Fal'ko, *Solid State Commun.* **2007**, *143*, 110.
[30] Y. Zhang, T. Tang, C. Girit, Z. Hao, M. C. Martin, A. Zettl, M. F. Crommie, Y. R. Shen, F. Wang, *Nature* **2009**, *459*, 820.
[31] K. Nakada, M. Fujita, G. Dresselhaus, M. S. Dresselhaus, *Phys. Rev. B* **1996**, *54*, 17954.
[32] O. Hod, J. E. Peralta, G. E. Scuseria, *Phys. Rev. B* **2007**, *76*, 233401.
[33] J. Campos-Delgado, Y. Kim, T. Hayashi, A. Morelos-Gómez, M. Hofmann, H. Muramatsu, M. Endo, H. Terrones, R. D. Shull, M. S. Dresselhaus, M. Terrones, *Chem. Phys. Lett.* **2009**, *469*, 177.
[34] X. Jia, J. Campos-Delgado, E. E. Gracia-Espino, M. Hofmann, H. Muramatsu, Y. A. Kim, T. Hayashi, M. Endo, J. Kong, M. Terrones, M. S. Dresselhaus, *J. Vac. Sci. Technol., B* **2009**, *27*, 1996.
[35] Y. C. Lin, C. Y. Lin, P. W. Chiu, *Appl. Phys. Lett.* **2010**, *96*, 133110.
[36] A. Das, S. Pisana, B. Chakraborty, S. Piscanec, S. K. Saha, U. V. Waghmare, K. S. Novoselov, H. R. Krishnamurthy, A. K. Geim, A. C. Ferrari and A. K. Sood, *Nat. Nanotechnol.* **2008**, *3*, 210.
[37] H. Medina, Y.-C. Lin, D. Obergfell, P.-W. Chiu. *Adv. Funct. Mater.* **2011**, *21*, 2687.
[38] D. Wei, Y. Liu, Y. Wang, H. Zhang, L. Huang, G. Yu, *Nano Lett.* **2009**, *9*, 1752.
[39] L. Qu, Y. Liu, J. B. Baek, L. Dai, *ACS Nano* **2010**, *4*, 1321.
[40] A. L. Elias, P. Ayala, A. Zamudio, M. Grobosch, E. Cruz-Silva, J. M. Romo-Herrera, J. Campos-Delgado, H. Terrones, T. Pichler, M. Terrones, *J. Nanosci. Nanotechnol.* **2010**, *10*, 3959.
[41] E. R. Alvizo-Paez, J. M. Romo-Herrera, H. Terrones, M. Terrones, J. Ruiz-Garcia, J. L. Hernandez-Lopez, *Nanotechnology* **2008**, *19*, 155701.
[42] T. Shimizu, J. Haruyama, D. C. Marcano, D. V. Kosinkin, J. M. Tour, K. Hirose, K. Suenaga, *Nat. Nanotechnol.* **2011**, *1*, 45.
[43] X. Jia, M. Hofmann, V. Meunier, B. G. Sumpter, J. Campos-Delgado, J. M. Romo-Herrera, H. Son, Y. Hsieh, A. Reina, J. Kong, M. Terrones, M. S. Dresselhaus, *Science* **2009**, *323*, 1701.
[44] J. M. Soler, E. Artacho, J. D. Gale, A. García, J. Junquera, P. Ordejón, D. Sánchez-Portal, *J. Phys.: Condens. Matter* **2002**, *14*, 2745
[45] J. P. Perdew, K. Burke, M. Ernzerhof, *Phys. Rev. Lett.* **1996**, *77*, 3865.
[46] V. Barone, O. Hod, G. E. Scuseria, *Nano Lett.* **2006**, *6*, 2748.
[47] S. Datta, *Quantum Transport: Atom to Transistor*, Cambridge University Press, Cambridge, UK **2005**.
[48] A. R. Botello-Mendez, E. Cruz-Silva, F. Lopez-Urias, B. G. Sumpter, V. Meunier, M. Terrones, H. Terrones, *ACS Nano* **2009**, *3*, 3606.
[49] V. Meunier, M. B. Nardelli, C. Roland, J. Bernholc, *Phys. Rev. B* **2001**, *64*, 195419.
[50] V. Meunier, M. B. Nardelli, J. Bernholc, T. Zacharia, J. C. Charlier, *Appl. Phys. Lett.* **2002**, *81*, 5234.
[51] J. M. Romo-Herrera, M. Terrones, H. Terrones, V. Meunier, *Nanotechnology* **2008**, *19*, 315704.
[52] L. Pisani, J. Chan, B. Montanari, N. Harrison, *Phys. Rev. B* **2007**, *75*, 064418.
[53] M. Brandbyge, J. L. Mozos, P. Odejon, J. Taylor, K. Stokbro, *Phys. Rev. B* **2002**, *65*, 165401.